Journal of Optoelectronics and Advanced Materials Vol. 6, No. 4, December 2004, p. 1133 - 1140

NANO-SCALE PHASE CHANGES IN Ge-Sb-Te FILMS WITH ELECTRICAL SCANNING PROBE MICROSCOPES

K. Tanaka*, T. Gotoh, K. Sugawara

Department of Applied Physics, Graduate School of Engineering, Hokkaido University, Sapporo 060-8628, Japan

Characteristics of amorphous-to-crystalline structural changes obtained using an electrical atomic force microscope and a scanning tunneling microscope have been investigated with simple models. A minimal mark size of ~10 nm is consistent with an empirical thermodynamic model. The mark size increases with electrical power and film thickness, which can be accounted for using thermal and crystal-growth models.

(Received September 29, 2004; accepted after revision November 29, 2004)

Keywords: Nano-scale phase change, Ge-Sb-Te, Crystallization, Scanning tunneling microscope, Atomic force microscope

1. Introduction

Continuous studies have been performed since the discovery of optical phase changes between amorphous and crystalline states in telluride films by Ovshinsky's group [1], and now we have a so-called re-writable DVD (digital versatile disk) system with a memory capacity of 50 GB per disk [2]. The system utilizes a blue laser with wavelength of 400 nm, which can write and erase one-bit marks of 150 nm in diameter. More advanced systems have already been explored [3-6], in which scanning near-filed optical microscopes or nonlinear optical films are utilized for producing smaller (~100 nm in diameter) crystalline marks in amorphous films. However, these mark sizes are still governed by the wavelength of laser light, and an ultimate material-limited mark has not been obtained by these optical systems.

To produce smaller marks, the electrical phase change [1,7] may be more promising, since the mark size can be reduced using smaller electrodes. Actually, several studies using small electrodes have already been done [8-12], in which the mark size is reduced to ~100 nm [9]. On the other hand, utilization of electrical atomic force microscopes (AFMs) and scanning tunneling microscopes (STMs) also seems to be interesting [13,14], since as is known these microscopes can provide atomic resolution [15]. Actually, very recently the authors have produced crystalline marks of ~10 nm and ~100 nm in diameter using an electrical AFM and an STM [16,17]. However, for understanding the nano-scale electrical phase change, it is necessary to investigate mark-formation mechanisms.

In the present work, therefore, we will consider the nano-scale electrical phase change characteristics using simple models. The AFM and STM results have been published separately [16,17], and accordingly, we briefly summarize the experiments and compare some results for discussion. We will also consider contrastive features of electrical and optical phase-change recordings.

2. Experiments

Fig. 1 shows AFM and STM experimental setups. In brief, samples had bilayer structures

*Corresponding author: keiji@eng.hokudai.ac.jp

consisting of amorphous $Ge_2Sb_2Te_5$ films [18] with thickness of 1 nm – 1 μm and metallic electrodes such as Au-Ni film or highly-oriented pyrolytic graphite (HOPG). The $Ge_2Sb_2Te_5$ films were prepared using a dc sputtering apparatus. For inducing electrical phase changes and mark probing, two commercial scanning probe microscopes (SPA-300, Seiko and Nanoscope E, DI) operating at 1 atm were employed with some modifications and peripherals such as external pulse generators. AFM cantilevers were prepared through depositing Au-Ni onto commercial Si_3N_4 probes (DNP-S, Veeco), and STM tips were made through electro-chemical etching of W wires. Phase changes were induced by applying pulse voltages of 1 – 10 V with duration of 5 ns - 1 ms to the sample through these metallic probes.

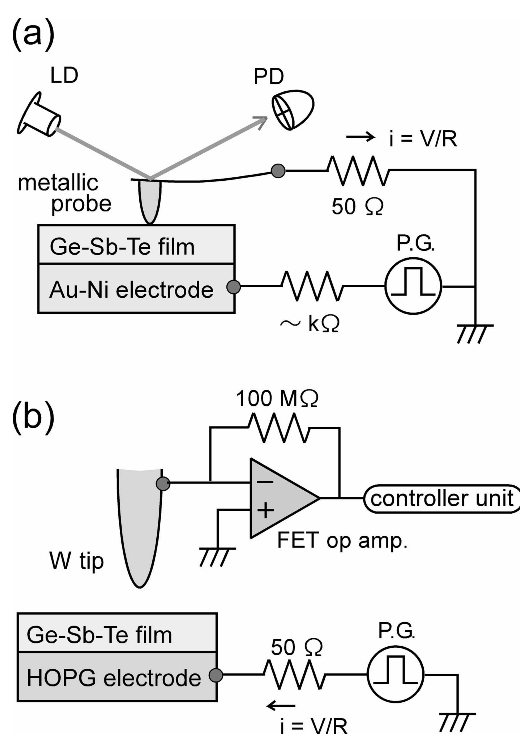

Fig. 1. Schematic illustrations of (a) an electrical AFM and (b) an STM for mark production. LD is an laser diode, PD a photodiode, P.G. a pulse generator. When probing marks, the pulse generator is replaced to a d.c. voltage supply.

3. Results

Fig. 2 compares the smallest crystalline marks obtained using the AFM and STM [16,17]. The AFM mark, which is imaged with a flowing current at a bias of 1 mV, is ~10 nm in diameter, in which we see facet-like faces. No topographic change has been detected for this mark. On the other hand, the STM mark is topographic, in which we see a doughnut-like deformation with outer diameter of ~100 nm. For larger marks of ~500 nm, we can obtain images using current-imaging tunneling spectroscopy, which manifest that the mark is electrically more conductive than peripheral amorphous regions. Note that these marks can be produced only when applied pulse voltages are higher than thresholds (see, Fig. 4).

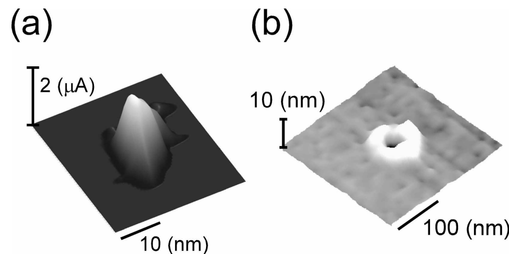

Fig. 2. (a) A current image of an AFM mark produced in a 1 nm-thick film with a pulse of 1 V, 1 mA, and 100 ns, and (b) a topographic image of an STM mark produced in 6 nm-thick film with a pulse of 3 V, a current smaller than 1 mA, and ~20 ns.

The electrical facet-like and the tunneling-spectroscopy image strongly suggest that the AFM and the STM mark are crystalline. Actually, using larger marks (0.5 - 50 μm), which were produced by applying higher and longer pulses to thicker films, structural changes from amorphous to crystalline have been detected using x-ray diffraction and Raman-scattering spectroscopy [16,17]. To the authors' knowledge, this is the first and direct (structural) demonstration of nano-scale electrical phase changes. Since the AFM mark is smaller and simpler in shape, it may be valuable to see the details first.

Mark stability should be noted at the outset. That is, 10 nm marks were unstable, disappearing with a single imaging scan with a probe voltage of 10 mV. However, the mark could be imaged at least after 1 h from the preparation. 20 nm marks gradually reduced the size with imaging scans, completely disappearing after three-times scans. 100 nm marks were more stable, while the size decreased to ~10 nm with a storage of ~3 h. These size reductions may be caused by some mark instability, film oxidation, and/or apex deterioration of the electrical AFM cantilevers. It should be mentioned here that the reversible phase change between amorphous and crystalline has been demonstrated for 50 nm marks [19].

Fig. 3 shows dependence of the mark diameter D upon the input electrical power P and the pulse duration τ. The films employed here are 10 - 25 nm in thickness. We see very roughly $D \propto P\tau^{1/2}$, which is similar to a feature obtained in an optical phase change [20].

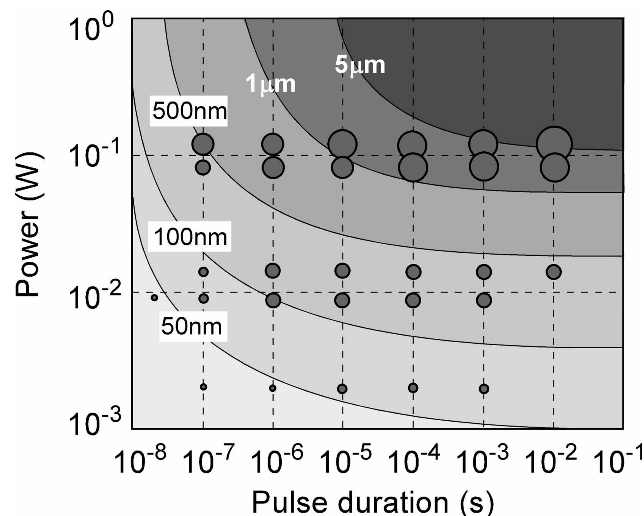

Fig. 3. Dependence of the mark diameter upon the input power and the pulse duration in films with thickness of 10 – 25 nm. The six kinds of circles represent the marks with approximate diameters of 30 nm, 70 nm, 200 nm, 700 nm, 2 μm, and 5 μm.

Fig. 4(a) shows dependence of the mark diameter D and threshold voltage V_t upon the film thickness L. The figure shows that, when $L < 5$ nm and $L > 5$ nm, $D \approx 10$ nm and $D \geq 2L$. Note that thinner films than 1 nm could not be inspected, due to rapid resistance increases (within ~10 min after film preparation), which probably suggested oxidation. On the other hand, we see that $V_t \propto L^{1/2}$. This result is contrastive to $V_t \propto L$, which is reported for $Te_{81}Ge_{15}Sb_2S_2$ films [1] and in the present STM experiment, as shown in Fig. 4(b) [17]. In the figure for the STM, we may also see $D \propto L$.

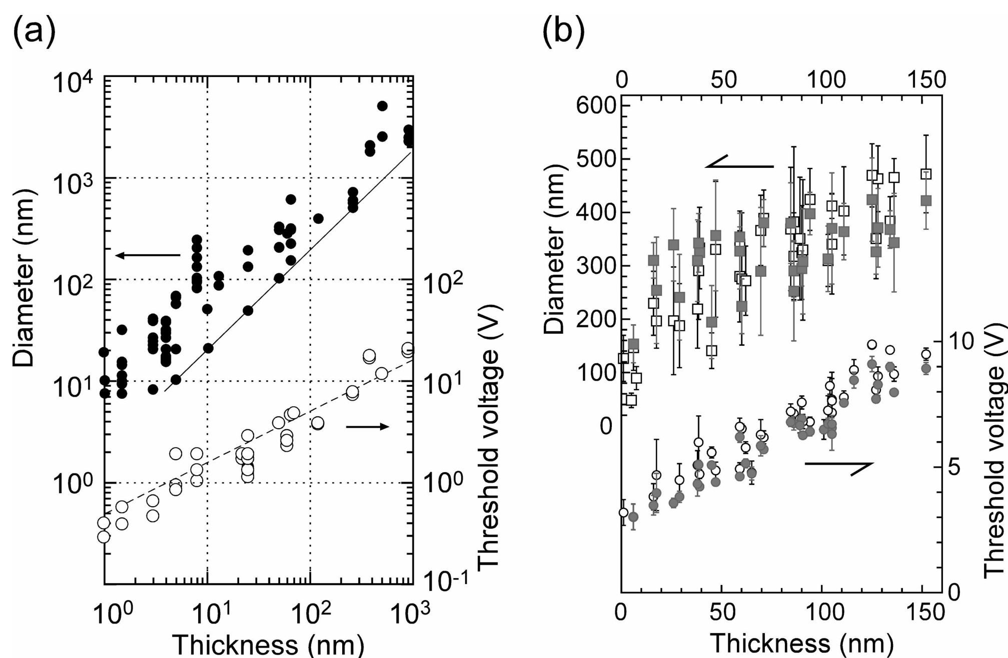

Fig. 4. Diameter and threshold voltage of AFM (a) and STM (b) marks as a function of the film thickness. Pulse voltage (also, current, and duration in (a)) is selected so that small marks can be produced. Note that the scales in (a) and (b) are logarithmic and linear.

4. Discussion

Mechanisms of electrical phase changes have not been elucidated, while it is assumed in general to be electro-thermal [7]. That is, when a pulse voltage is applied to a semi-insulating amorphous sample, a so-called *conducting channel* is formed between electrodes through some electronic process such as avalanche breakdown or trap filling [7]. Then, a high current flows through the channel, which generates Joule heats, rising the channel temperature above the crystallization threshold, which is ~140 °C in $Ge_2Sb_2Te_5$ [21]. Crystal nucleation and growth occur under this heated condition, which will continue until the pulse voltage is terminated.

The relation $V_t \propto L^{1/2}$ in Fig. 4(a) can be explained very simply. We assume that the shape of the conducting channel is cylindrical with a cross-sectional area of S and a length, which is equal to the film thickness L (see, Fig. 5). The electrical power P is fed into the volume of SL, so that the temperature rise ΔT can be written as $P \propto SL\,\Delta T$, where heat dissipation is neglected in a very initial stage. Since $P \propto V_t^{\,2}$, provided that S is independent of L and V_t, we obtain $V_t \propto L^{1/2}$, which is consistent with the observation.

Under the heated condition, the crystal growth is assumed to start at the probe-film contact (see, Fig. 5). This is because the sharp apex can generate a hemi-spherical electric field with the origin at the contact, which will trigger the conducting-channel formation and temperature rise. The apex must also exert some strains, which may assist crystallization [22]. In contrast, since the sample is deposited onto metallic electrodes on glass substrates, having greater thermal capacity, the sample-electrode interfacial temperature tends to rise more slowly. These features possibly cause

crystallite nucleation and successive growth at and from the probe-film contact.

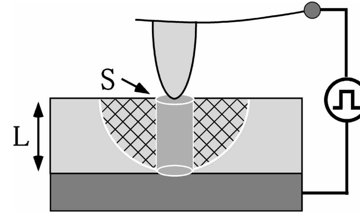

Fig. 5. A schematic illustration of a conducting channel and a hemispherical crystallite with a radius being equal to the film thickness.

The above assumption can explain the observed relation $D \geq 2L$ in Fig. 4(a). That is, we can assume that the crystal grows hemi-spherically, and when the crystal front reaches to the bottom electrode, as illustrated in Fig. 5, the growth will be quenched with a sudden temperature drop due to large thermal conductivity and capacity of the metal electrode and substrates. The growth kinetics must change at this instance from three- to two-dimensional, which may also suppress the growth rate [23]. Accordingly, the minimal mark diameter becomes to be seemingly $2L$.

Alternatively, we may assume that the relation arises as a result of AFM measurements. That is, smaller marks might be produced, while if the crystalline mark originating from the probe-film interface does not reach the bottom electrode, the electrical AFM measurement cannot detect the mark due to higher resistance of remaining amorphous layer. Then, the diameter of minimal and detectable marks becomes to be $2L$. However, since the cylindrical electrically-conducting channel must exist through the film thickness and the crystallization is an exo-thermal reaction, it is difficult to envisage that the hemispherical crystal growth stops in a half way. In addition, the AFM has substantial accuracy in d.c. current measurements, and accordingly, this possibility can be ignored.

On the other hand, for the ultimate mark diameter of ~10 nm, several interpretations may be possible. For instance, it may be governed by the curvature size of cantilever apex, which can be estimated at ~50 nm, which gives a nominal diameter of contact areas of ~0.5 nm [16]. Otherwise, the mark size may be related with the conducting channel diameter.

A thermo-dynamical model can provide a quantitatively plausible explanation for the minimal mark size [24]. A spherical crystal with a radius of r grown in an amorphous network changes the free energy by ΔG, which can be expressed as

$$\Delta G = - (4/3)\, \pi\, r^3\, \Delta G_V + 4\, \pi\, r^3\, d\, \Delta G_S\,,$$

where the suffices V and S indicate volumeric and interfacial contributions, and d is an interfacial layer thickness. Then, we see that the two conditions are needed for a crystal growth at around the crystallization temperature T_c. One is $r > r_c$ for the critical radius r_c = 2d $\Delta G_S / \Delta G_v$, and the other is $E_B > kT_c$ for the barrier height $E_B = (16/3)\, \pi\, d^3\, \Delta G_S^3 / \Delta G_V^2$. We here tentatively assume that $\Delta G_S \approx \Delta G_V$, since it is difficult to estimate ΔG_S. In addition, we can envisage $d = 1 \sim 3$ nm from two kinds of studies. That is, in an experiment on chalcogenide multi-layers [25], when a layer thickness becomes smaller than 1 - 2 nm, the multi-layer structure disappears. This result implies that 1 - 2 nm is a minimal thickness needed for producing interfacial structures. We also note, e.g., Refs. 26 and 27, which show that the interfacial layer thickness of amorphous SiO_2 on crystalline Si is a few nm. Then, using these values, we obtain very roughly $2r_c \approx 10$ nm, which is consistent with the observed minimal mark size. This size may also be consistent with the observed instability of small (10 - 50 nm) marks. It should be mentioned here that the minimal size of ~10 nm is reported also in other structural changes produced at room temperature [28-30], to which the present model can be applied with some modifications.

If the input electrical power P is greater and the pulse duration τ is longer, the crystal growth will continue after reaching to the bottom electrode. Or, as shown in Fig. 1(b) in Ref. 16, nucleation-type crystallization appears in a region, where temperature is higher than the crystallization temperature. In this case, the temperature distribution, which can be calculated from the heat-diffusion equation, is important. A simple analysis shows that the radius r of heated circular

disk increases with $r \propto P\,\tau^{1/2}$, which is actually demonstrated for optical phase changes [20]. This proportionality is consistent with the present observations in Fig. 3. We can conclude therefore that, upon high energy input, the electrical and the optical crystallization give similar features.

In STMs, as illustrated in Fig. 6, the existence of tunneling gaps is essential. When a pulse voltage of ~5 V is applied to a tunneling gap through an STM tip, an electric filed of 10^7 V/cm (or 10^6 V/cm) is applied to the gap between an STM tip and the film surface (or the electrode surface provided that the amorphous film is insulating). Then, the tip elastically elongates due to Coulombic attraction by ~10 nm [17,31]. A simple mechanical analysis using an estimated tip mass suggests that the elongation occurs with a time constant of ~10 ns, which may be compatible with observed electrical transients [17]. It is reasonable to assume that the minimal threshold voltage, ~3 V (Fig. 4(b)), corresponds to the tip elongation which terminates the tunneling gap. As illustrated in Fig. 6(b), the tip may intrude into the film with some inertia or the tip-electrode force, making an electrical contact. This insertion is assumed to be responsible for the doughnut-like deformation shown in Fig. 2(b). Afterwards, in similar ways to those in the AFM case, the conducting-channel formation and crystallization process follows.

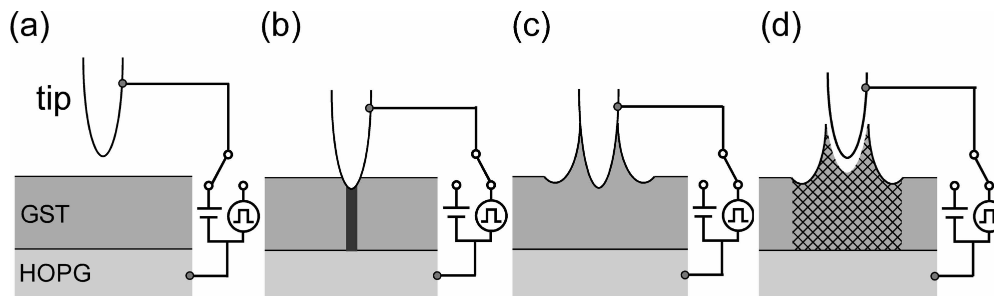

Fig. 6. Transients of STM crystallization.

It is noted that phase changes by tunneling currents have not been attained due to limited flowing currents. Upon application of 1 V to a tunneling gap of 1 nm, which is a typical STM imaging condition, a tunneling current between an STM tip and a metal surface is practically ~μA [15]. Since an amorphous $Ge_2Sb_2Te_5$ is semi-insulating (10^{-3} S/cm), the current still decreases. This current level is smaller by several orders than that (~mA) needed for Joule heating up to the crystallization temperature in the present experimental condition [17]. On the other hand, if we may increase the voltage to ~10 V, a high electric field existing at the tunneling gap is liable to induce field effects such as electro-chemical reaction and field evaporation [32-34].

5. Comparison and summary

Comparing these AFM and STM characteristics in the present work, we can conclude that AFMs are more suitable to electrical nano-scale phase changes. In the present STM, the tip intrudes into the film when a voltage is higher than ~3 V, and accordingly, the tip necessarily gives drastic effects upon the film. Since fast (~ns) control of the tip motion is more-or-less difficult, the STM with a metallic tip seems to be less appropriate for producing small marks. Otherwise, it will be an interesting challenge to employ STMs with flexible and shape-controlled tips.

Finally, it seems to be valuable to compare some characteristics of optical and electrical phase changes. In the present work, we have mainly dealt with the mark size, which governs the memory capacity. However, another important key factor of the phase-change recording is the response time, which includes writing, erasing, and reading times. Here, it is known that the crystallization, which is the erasing process in commercial DVDs, needs the longest time.

Fig. 7 summarizes a historical overview of the phase-change recordings in the bit size and the response speed. In the Ovshinskys' era, when films such as $Te_{81}Ge_{15}Sb_2S_2$ were employed, a bit size was a few microns, but slow response time of μs - ms was very problematic in practical usage. Then, Yamada et al. has demonstrated that such slow response in the amorphous-to-crystalline phase change is caused by long-range atomic diffusion leading to phase-separated crystalline

structures in the non-stoichiometric film [21]. They also discovered a new system, quasi-binary $GeTe-Sb_2Te_3$, which has response time of 10 - 50 ns due to short-range atomic migrations upon crystallization. In addition, red or blue semiconductor lasers with combination of a high numerical-aperture focussing-lens have reduced the one-bit size to 400 - 150 nm [2].

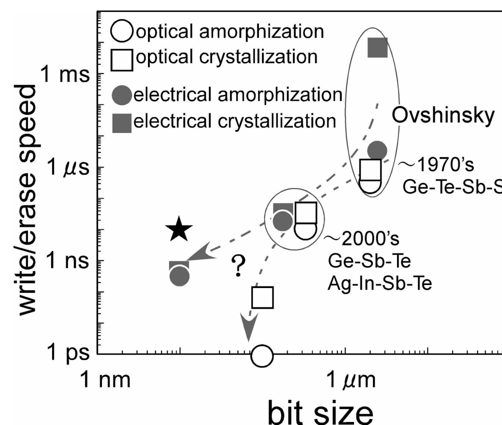

Fig. 7. Historical development of response time and mark size of electrical and optical phase-change recordings. The star shows the present AFM crystallization.

Then, what is the future? We believe that the optical and the electrical system will develop toward different extremes. As is demonstrated in the present work, the electrical system can produce 10 nm marks, while electrical circuits possess an intrinsic response time limit of ns to sub-ns, which is governed by stray capacitance. On the other hand, in the optical system, the light wavelength will pose a mark-size limit at ~100 nm, provided that evanescent optical systems could be employed [3-5]. However, we already have ps - fs lasers, and some studies have demonstrated that ultra-short laser pulses can produce some phase changes [35,36]. Although such observations do not necessarily suggest that the phase change is completed within ps time scales, the study implies some possibility of ultra-fast operation. We may then predict that the phase change will provide a dramatic progress in memory devices, which started from the Edison's record about a century ago.

References

[1] S. R. Ovshinsky, H. Fritzsche, IEEE Trans. **ED-20,** 91 (1973).
[2] Panasonic homepage, http://matsushita.co.jp/corp/news/official.data/data.dir/en040630-5/en0406305.html.
[3] S. Hosaka, T. Shintani, M. Miyamoto, A. Kikukawa, A. Hirotsune, M. Terao, M. Yoshida, K. Fujita, S. Kämmer, J. Appl. Phys. **79**, 8082 (1996).
[4] J. Tominaga, T. Nakano, and N. Atoda, Appl. Phys. Lett. **73**, 2078 (1998).
[5] K. Kishima, I. Ichimura, K. Saito, K. Yamamoto, Y. Kuroda, A. Iida, S. Masuhara, K. Osato, Jpn. J. Appl. Phys. **41,** 1894 (2002).
[6] K. Furihara, K. Nanri, K. Toto, Appl. Phys. Lett. **84,** 3415 (2004).
[7] A. Madam, M. P. Shaw, The Physics and Applications of Amorphous Semiconductors (Academic Press, Boston, 1988) Chap. 5.
[8] S. R. Ovshinsky, Romanian Rept. Phys. **51,** 171 (1999).
[9] H. Tanaka, T. Nishihara, T. Ohtsuka, K. Morimoto, N. Yamada, K. Morita, Jpn. J. Appl. Phys. **41**, L1443 (2002).
[10] J. D. Maimon, K. K. Hunt, L. Burcin, J. Rogers, IEEE Trans. Nuclear Sci. **50,** 1878 (2003).
[11] K. Nakayama, K. Kojima, Y. Imai, T. Kasai, S. Fukushima, A. Kitagawa, M. Kumeda, Y. Kakimoto, M. Suzuki, Jpn. J. Appl. Phys. **42**, 404 (2003).
[12] D. H. Kang, D. H. Ahn, K. B. Kim, J. F. Webb, K. W. Yi, J. Appl. Phys. **94,** 3536 (2003).
[13] H. Kado, T. Tohda, Jpn. J. Appl. Phys. **36**, 523 (1997).

[14] D. Saluel, J. Daval, B. Béchevet, C. Germain, B. Valon: J. Magn. Magn. Mater. **193,** 488 (1999).
[15] R. Wiesendanger, J. Vac, Sci. Technol. **B12,** 515 (1994).
[16] T. Gotoh, K. Sugawara, K. Tanaka, Jpn. J. Appl. Phys. **43,** L818 (2004).
[17] K. Sugawara, T. Gotoh, K. Tanaka, Jpn. J. Appl. Phys. **43,** L676 (2004).
[18] Note that the average coordination number of this material is 2.67, provided that the 8-N rule applies to Ge, Sb, and Te.
[19] T. Gotoh, K. Sugawara, K. Tanaka, J. Non–Cryst. Solids **299–302**, 968 (2002).
[20] V. Weidenhof, I. Friedrich, S. Ziegler, M. Wuttig, J. Appl. Phys. **89**, 3168 (2001).
[21] N. Yamada, E. Ohno, K. Nishiuchi, N. Akahira, M. Takao, J. Appl. Phys. **69,** 2849 (1991).
[22] K. Tanaka, J. Non-Cryst. Solids **150,** 44 (1992).
[23] Z. Fan, D.E. Laughlin, Jpn. J. Appl. Phys. **42,** 800 (2003).
[24] K. Tanaka, J. Non-Cryst. Solids **326**, 21 (2003).
[25] E. Vateva, D. Nesheva, J. Non-Cryst. Solids **191,** 205 (1995).
[26] M. C. Cheynet, T. Epicier, Philos. Mag. **84**, 1753 (2004).
[27] K. Tatsumura, T. Watanabe, D. Yamasaki, T. Shimura, M. Umeno, I. Ohdomari, Jpn. J. Appl. Phys. **43,** 492 (2004).
[28] Y. Utsugi, Nature **347**, 747 (1990).
[29] A. Sato, Y. Tsukamoto, Nature **363,** 431 (1993).
[30] B. J. Kooi, W. M. G. Groot, J. Th. M. De Hosson, J. Appl. Phys. **95,** 924 (2004).
[31] U. Gratzke, G. Simon, Phys. Rev. **B52,** 8535 (1995).
[32] K. Sugawara, T. Gotoh, K. Tanaka, Appl. Phys. Lett. **79**, 1549 (2001).
[33] M. Ohto, K. Tanaka, J. Appl. Phys. **92,** 5468 (2002).
[34] K. Sugawara, T. Gotoh, K. Tanaka, J. Non–Cryst. Solids **326–327,** 37 (2003).
[35] T. Ohta, J. Optoelectron. Adv. Mater. **3,** 609 (2001).
[36] J. Siegel, A. Schropp, J. Solis, C.N. Afonso, M. Wuttig, Appl. Phys. Lett. **84,** 2250 (2004).